



Information Entropy for a Two-Dimensional Rotating Bose–Einstein Condensate

R. Kishor Kumar¹ · B. Chakrabarti¹ · A. Gammal¹

Received: 15 March 2018 / Accepted: 2 August 2018
© Springer Science+Business Media, LLC, part of Springer Nature 2018

Abstract

We study the information entropy, order, disorder, and complexity for the two-dimensional (2D) rotating and nonrotating Bose–Einstein condensates. The choice of our system is a complete theoretical laboratory where the complexity is controlled by the two-body contact interaction strength and the rotation frequency (Ω) of the harmonic trap. The 2D nonrotating condensate shows the complexity of the category I where the disorder–order transition is triggered by the interaction strength. In the rotating condensates, Ω is chosen as the disorder parameter when the interaction strength is fixed. With respect to Ω , the complexity shifts between maximum and minimum confirm the existence of category II complexity in the rotating condensate. Also, we consider the interaction strength as the disorder parameter when Ω is unchanged and complexity as a function of interaction strength exhibits category III complexity. The present work also includes the calculation of upper bound and lower bound of entropy for 2D quantum systems.

Keywords Bose–Einstein condensate · Vortex lattice · Information entropy

1 Introduction

Information theory plays an important role in the study of quantum systems, and it has been successfully used in the analysis of electron densities in atoms and molecules [1–7]. The information theoretical approach of entropy maximization was applied in the analysis of Compton profiles and electron momentum distributions [1,2]. Also, the interpretation of quantum information theory is essential for quantum optics and condensed matter physics in the information transmission and computation [8]. The measurements of the observable in quantum experiment help to analyze the quantum systems and provide information about the state of the system. Importantly, mea-

✉ R. Kishor Kumar
kishor@if.usp.br

¹ Instituto de Física, Universidade de São Paulo, São Paulo 05508-090, Brazil

measurements of entropy may help to identify the nonequilibrium state of the quantum system.

The universal trend of the information entropy both for fermions and bosons is an important observation for the study of quantum mechanical systems [9–11]. Information entropy is calculated using one-body density in position space (S_r) and in momentum space (S_k) obeys same approximate functional form $\sim a + bN^{1/3}$, (where N is the number of particles) universally for all types of quantum many-body systems. The net information entropy is also an increasing function of N . A simple functional form $S = a + b \ln N$ holds approximately for atoms, nuclei, atomic clusters, and correlated bosons in a trap. An important step in this direction is the discovery of entropic uncertainty relation (EUR) for a three-dimensional (3D) system $S_r + S_k \geq 3(1 + \ln \pi) \cong 6.434$ ($\hbar = 1$) [4,6,12]. The lower limit is attained for the noninteracting model when the distribution is Gaussian. A direct connection between information entropy and kinetic energy for the quantum many-body system is also established [13–15]. The total entropy is an increasing function of the number of particles in the system, independently of whether the system is an atom or a nucleus (as in references [13,14]). Recently, it has been observed that for K-shell electrons of atoms the total correlated entropy decreases as one goes along the periodic table [16,17]. However, order, disorder, and complexity are the three important measures which are inherently connected with the measure of entropy. We note that concepts of entropy and disorder are decoupled in most of the applications [9–11,18,19]. When entropy increases, the Landsberg order parameter also increases and it was concluded that a simultaneous increase in entropy and order can be explained if entropy and disorder are decoupled [20,21]. It has also been explicitly shown for N trapped dipolar Bose gas that order and entropy increase simultaneously [19]. The recent theoretical observation explained that the total entropy of the Bose gas in the 3D trap is associated with the atoms in an excited state, although the entropy of particles in the ground state is nonzero [22].

The investigation of rotating Bose–Einstein condensate is one of the central topics in the study of ultracold quantum physics due to its interesting features that includes an array of orderly aligned lattices in the quantum-Hall regime, Tkachenko oscillations in the lowest Landau level, bending of vortex lines, and so on, which can be traced by several review papers and books on the subject (as references in [23–27]). The vortices are observed in experiments by quantum engineering techniques based on the atom-field coupling [28], topological phase manipulation [29], with synthetic magnetic fields [30], and rotating the magnetic trap [31,32]. Following the experiments, several theoretical investigations have been made to study the properties of BECs including vortices [33–38]. In particular, the imaginary-time propagation method is used to generate the stationary vortices [33,34]. Also, studies beyond mean-field are carried out to observe the fragmentation due to rotation using multi-configurational Hartree method for bosons [39].

Complexity measure is an ideal quantity that can serve as an ideal parameter to quantify the complex behavior of the different quantum systems. Various definitions of complexity exist in the literature [18,40–42]. Two simple measures of complexity are López-Ruiz, Mancini, and Calbet (LMC) [43] and Shiner, Davison, and Landsberg (SDL) [18]. However, the alternative definition of complexity $\Gamma_{\alpha\beta}$ is defined by SDL

measure which is based on the appropriately defined notions of order and disorder [18]. SDL defined the order parameter $\Lambda = 1 - \frac{S}{S_{\max}}$, where S is the total information entropy and S_{\max} is the maximum entropy accessible to the system. At $\Lambda = 0$, the system is at maximum accessible entropy with $S = S_{\max}$ and exhibits completely disordered state. On the other hand, $\Lambda = 1$ implies that the system is at zero entropy and corresponds to perfect ordered state. For a realistic system, Λ lies between zero and one. The SDL measure $\Gamma_{\alpha\beta}$ broadly classifies three categories of complexity as a function of the disorder [18,44]. In category I, complexity is a monotonically increasing function of the disorder. In category II, complexity is minimum both for perfect order and perfect disorder, exhibits a maximum at the intermediate level of disorder. In the category III, complexity is a monotonically decreasing function of the disorder. However, we follow the simplest measure of complexity $\Gamma = \Delta(1 - \Delta)$ [18].

In this paper, we calculate the information entropy, order, disorder, and complexity for the 2D rotating and nonrotating BECs. The justification of the choices of the system: (a) it is an experimentally achievable highly complex system; (b) the interaction strength and the rotational frequency can both serve as a disorder parameter; and (c) higher rotation frequencies may lead to the system to nonequilibrium when many vortices are developed. Thus, this is the most attractive test bed for studying the complexity, order-disorder transition and also to justify whether the usual thermodynamical picture will be valid, i.e., order and entropy are coupled. It facilitates two separate phases for the study of complexity. In the first phase, we considered the nonrotating condensates and observed the category I complexity [18]. In the second phase, the rotating condensate is considered to study the categories of complexity. The rotation frequency is considered as a disorder parameter when the interaction strength is unchanged. The complexity for rotating condensate is minimum both for perfect order and disorder, also, it exhibits a hump at some critical rotation frequency ($\Omega = \Omega_c$) evidences a category II type of complexity in the rotating condensate [18]. For the rotating condensate with the fixed rotation frequency, complexity has now decreased with increase in interaction strength (disorder parameter). It exhibits category III complexity. For the study of the order-disorder transition, one must have all the fundamental relations of entropy lower bound and upper bound on the conjugate space in two dimensions. So, we derive the fundamental inequalities for 2D quantum systems [14].

The paper is organized as follows. In Sect. 2, we present the 2D mean-field model for the trapped BEC under rotation, numerical methods used and quantities of interest of this work. In Sect. 3, we report entropy calculations for nonrotating and rotating BECs by varying the contact interaction strength and rotation frequency. The paper is concluded in Sect. 4.

2 Formalism

At ultra-low temperatures, the properties of a Bose–Einstein condensate of N atoms, each of mass m , in rotating frame can be described by the 3D mean-field Gross–Pitaevskii (GP) equation [23]. The external trapping potential is provided by the usual 3D harmonic trap, with a strong pancake-shaped symmetry and corresponding trap

aspect ratio λ . A strong pancake-shaped trapping potential, V_{trap} , is assumed to be of the form

$$V_{\text{trap}}(\mathbf{r}) = \frac{1}{2}m\omega^2(x^2 + y^2 + \lambda^2z^2),$$

where m and ω are the mass and trap frequency, respectively.

For the present study, we assumed pancake-shaped trap with $\lambda = 10$. So, we reduce the corresponding 3D equation to a two-dimensional form by assuming the usual factorization of the wave function into the ground state of the transverse harmonic oscillator trap and a 2D wave function

$$\Psi(\mathbf{r}, t) \equiv \left(\frac{\lambda}{\pi l^2}\right)^{1/4} \exp\left(\frac{-\lambda z^2}{2l^2}\right) \times \Psi_{2\text{D}}(x, y, t). \quad (1)$$

We performed the 2D reduction by introducing the above ansatz in the original 3D GP formalism. The final equation is in a dimensionless form where energy in units of $\hbar\omega$, length in units of $l = \sqrt{\hbar/(m\omega)}$, and time is given in units of $\tau = 1/\omega$. The dimensionless wave-function component is given by $\Psi(x, y, \tau) \equiv l\Psi_{2\text{D}}(x, y, t)$. The corresponding 2D equation

$$i\frac{\partial\Psi_{2\text{D}}(x, y, t)}{\partial\tau} = \left[-\frac{\nabla_{x,y}^2}{2} + V(x, y) - \Omega L_z + g_{2\text{D}}|\Psi_{2\text{D}}(x, y, t)|^2\right]\Psi_{2\text{D}}(x, y, t), \quad (2)$$

where $V(x, y) = \frac{x^2+y^2}{2}$ is the external harmonic trap, $g_{2\text{D}} = 2\sqrt{2\pi\lambda}\frac{aN}{l}$ is the contact interaction parameter, N is the number of atoms, and a is the two-body atomic scattering length. $L_z = -i\hbar(x\partial_y - y\partial_x)$ is the angular momentum operator with Ω the corresponding rotation frequency (in units of ω).

For the numerical solution of Eq. (2), we employ the split-step Crank–Nicolson method, as in Refs. [45–49]. The numerical simulations are carried out in imaginary-time propagation on a grid with 512 points in x and y directions, spatial steps $\Delta x = \Delta y = 0.05$ and time step $\Delta t = 0.0005$. The wave function is renormalized to $\int dx dy |\Psi_{2\text{D}}|^2 = 1$ after each time step. Also, the convergence of vortex solution is confirmed by conjugate gradient method [50,51]. As found appropriate for experimentally realistic settings, in all the following analysis we are taking a pancake-shaped trap, with an aspect ratio $\lambda = 10$.

To calculate the stationary vortex states, the different initial guesses are used to check the convergence of ground state. From the tests, we choose the following suitable initial conditions in the form of a combination of angular harmonics [52],

$$\Psi_{2\text{D}}(x, y) = \sum_{m=0}^L \frac{(x+iy)^m}{\sqrt{\pi(L+1)m!}} \exp\left[-\left(\frac{x^2+y^2}{2}\right)\right] \exp(i2\pi\mathcal{R}_m), \quad (3)$$

where \mathcal{R}_m is a randomly generated number uniformly distributed between 0 and 1, with arbitrary integer value for L that we have considered up to $L = 100$.

2.1 Quantities of Interest : Entropy, Order, Disorder, and Complexity

For a three-dimensional system with the continuous probability distribution $n(\mathbf{r})$ in position space, the information entropy S_r is calculated from

$$S_r = - \int n(\mathbf{r}) \ln n(\mathbf{r}) d\mathbf{r}, \quad (4)$$

where $n(\mathbf{r}) = |\Psi(\mathbf{r})|^2$ is the one-body density and the corresponding information entropy in momentum space S_k is calculated as

$$S_k = - \int n(\mathbf{k}) \ln n(\mathbf{k}) d\mathbf{k}, \quad (5)$$

where $n(\mathbf{k}) = |\tilde{\Psi}(\mathbf{k})|^2$ is the density distribution in the momentum space, and the momentum space wave function $\tilde{\Psi}(\mathbf{k})$, can be obtained from the fast Fourier transform of $\Psi(\mathbf{r})$. Both the density distributions $n(\mathbf{r})$ and $n(\mathbf{k})$ are normalized to one. In this case, we calculate the entropy per particle until it becomes a constant that depends on $\ln N$ [10]. It is noted that entropy measures are scale invariant to the uniform change of coordinates. For the 3D system, the rigorous relation between S_r and S_k , total kinetic energy (T) and mean square radius has been derived using the EUR and they are presented by three inequalities [14,15],

$$S_{r\min} \leq S_r \leq S_{r\max}, \quad (6)$$

$$S_{k\min} \leq S_k \leq S_{k\max}, \quad (7)$$

$$S_{\min} \leq S \leq S_{\max}. \quad (8)$$

To calculate the above measures in two dimensions, we need the expressions for the lower and upper bounds like $S_{r\min}$, $S_{r\max}$, $S_{k\min}$, $S_{k\max}$, S_{\min} , and S_{\max} . We follow the same technique from Ref. [14] and derive the upper and lower bound entropy equations for 2D quantum system. These inequality relations are presented in ‘‘Appendix,’’ which are further utilized for the calculation of order $\Delta = 1 - \frac{S}{S_{\max}}$, disorder $\Delta = \frac{S}{S_{\max}}$, and complexity $\Gamma = \Delta(1 - \Delta)$ for the 2D rotating and nonrotating condensates.

3 Results

We start by considering a nonrotating case in Sect. 3.1. Next, we consider the rotating BEC in Sect. 3.2. All the following results are produced with the parameter of the contact interaction is given in units of the Bohr radius a_0 . Adopting the length unit

as $l = 1.89 \times 10^4 a_0$, the coordinates and densities are presented as dimensionless quantities.

3.1 Nonrotating BECs (Category I Complexity)

We calculate the total entropy by solving the two-dimensional GP Eq. (2) numerically for $\Omega = 0$ and various interaction strengths g_{2D} . The information entropy S_ρ for the 2D density distribution is calculated by

$$S_\rho = - \int n(\rho) \ln n(\rho) d\rho, \quad (9)$$

where $n(\rho) = |\tilde{\Psi}_{2D}(\rho)|^2$ is the 2D density and $\rho \equiv (x, y)$. Also, the corresponding density in momentum space $n(\mathbf{k}_\rho)$ is obtained from the fast Fourier transform (FFT) and S_{k_ρ} is calculated by using Eq. (10) which is presented in ‘‘Appendix.’’ The total entropy ($S = S_\rho + S_{k_\rho}$), upper bound (S_{\max}), and lower bound (S_{\min}) are plotted in Fig. 1. The total entropy S of the nonrotating condensate perfectly lies between S_{\max} and S_{\min} throughout the entire range of interaction strength. The used inequality expressions to calculate the upper and lower bounds of entropy are given in Appendix Eq. (17). Further, we have calculated the corresponding Landsberg order parameter, disorder, and complexity in Fig. 2. In Fig. 2a, order increases regarding the increase in interaction strength g_{2D} (which is proportional to a number of particles), and then order saturates. We observe that order and entropy both increase as similar to the previous observation of 3D condensate [11,19]. This is confirming the explanation; order and entropy are decoupled. The corresponding measure of disorder $\Delta = (1 - \Lambda)$ smoothly decreases and attains a saturation. From the above observations, we confirm that adding more particles to the system manifests the transition from disorder to order. In Fig. 2c, we plot the complexity $\Gamma = \Delta(1 - \Delta)$, which increases monotonically against disorder parameter g_{2D} and then saturates. Thus, our nonrotating 2D condensate exhibits complexity which belongs to the category I [18]. The saturation of the order, disorder, and complexity at a critical interaction strength $g_{2D} \approx 330$ can observe from Fig. 2.

3.2 Rotating BECs (Category II and III Complexity)

In this subsection, we consider the 2D rotating BECs and investigate its entropy properties. The vortex lattice is obtained by propagating the 2D GP equation (2) in imaginary time with nonzero rotation frequency Ω . The first vortex appears at a rotation frequency significantly larger than critical frequency Ω_c for the vortex generation. The vortex lattice is strongly influence by the trap symmetry [33,34]. In Fig. 3, we display the stable solutions for densities showing the triangular vortex lattice for different interaction strengths and rotation frequencies. Saturation in the order, disorder, and complexity is the effect of the external finite sized trap. This critical interaction strength crucially depends on the trap aspect ratio.

Fig. 1 Entropy measure of 2D nonrotating condensate. Upper (S_{\max}) and lower (S_{\min}) limits of entropy are compared with the total entropy (S) of the condensate with respect to interaction strengths. S_{\max} , and S_{\min} are represented by solid lines with solid stars, triangles, and circles, respectively. All quantities are dimensionless (Color figure online)

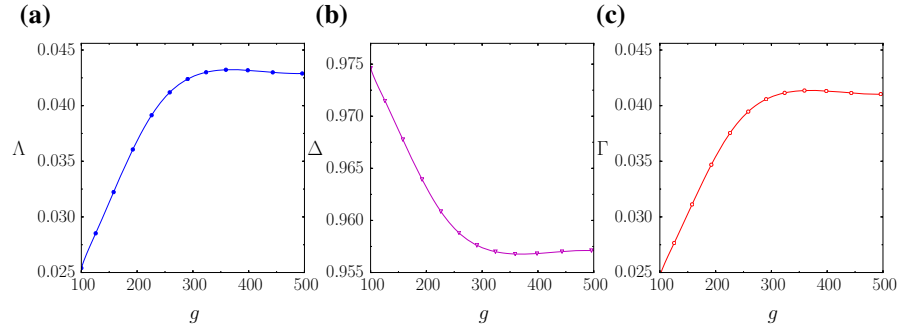
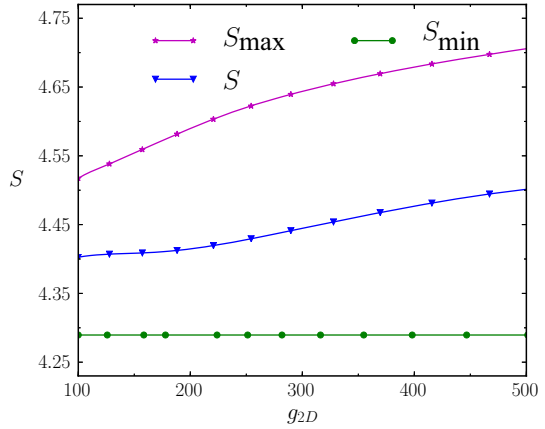


Fig. 2 In the upper, middle and lower panels, **a** order, **b** disorder and **c** complexity of the nonrotating condensate as a function of interaction strengths are shown, respectively. The smooth increase in Λ (**a**) corresponding smooth decrease in Δ (**b**) and characterized category I complexity in (**c**). All quantities are dimensionless (Color figure online)

In Fig. 4, we present the number of vortices (N_v), expectation value of the angular momentum of the condensate ($\langle L_z \rangle$), and total entropy (S) as a function of rotation frequency. The N_v , $\langle L_z \rangle$, and S all three parameters are increasing with respect to Ω . The number of vortices and angular momentum diverge at the rotation frequency near to harmonic trap frequency [52]. But the entropy of the system increases smoothly as shown in Fig. 4c. There is a discontinuous transition between N_v and $\langle L_z \rangle$ both jump from zero to unity when the first vortex enters. Similarly, there is a jump in the total entropy, when the first vortex enters into the condensate. The discontinuous increase in N_v , $\langle L_z \rangle$ and S with increasing Ω is due to the dynamical entry of vortices into the condensate. The angular momentum essentially depends on the number of vortices, but it does not fluctuate significantly by the orientation of the condensate regarding the vortex lattice arrangement and radius of the condensate. So, the angular momentum does not increase significantly. But total entropy remains the same if the number of vortices is unchanged. So, between some rotation frequencies, the angular momentum goes up continuously, while entropy may rise discontinuously. This difference can be visualized by comparing Fig. 4b, c. Next, the upper limit (S_{\max}), lower limit (S_{\min}) of

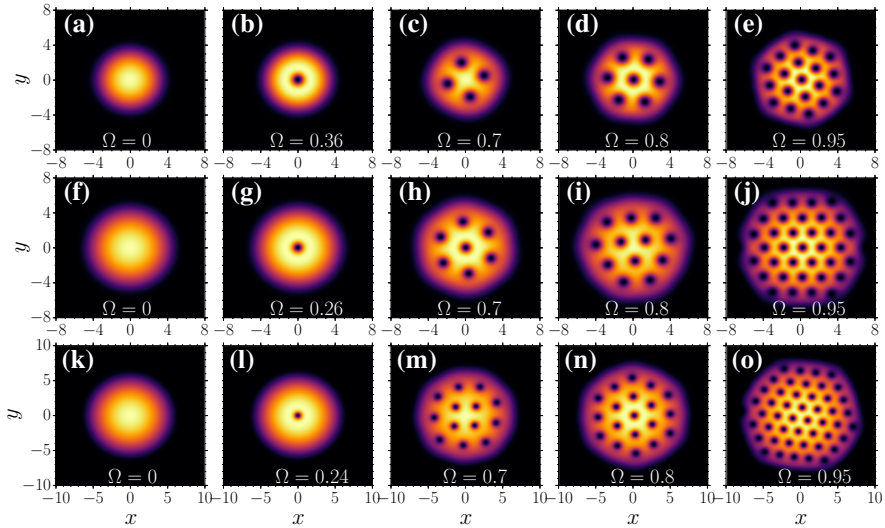


Fig. 3 Two-dimensional density patterns, $|\Psi_{2D}|^2$ for the interaction parameters **a–e** $g_{2D} = 100$, **f–j** $g_{2D} = 250$, and **k–o** $g_{2D} = 500$. The corresponding rotation frequency is mentioned in each density plot (Color figure online)

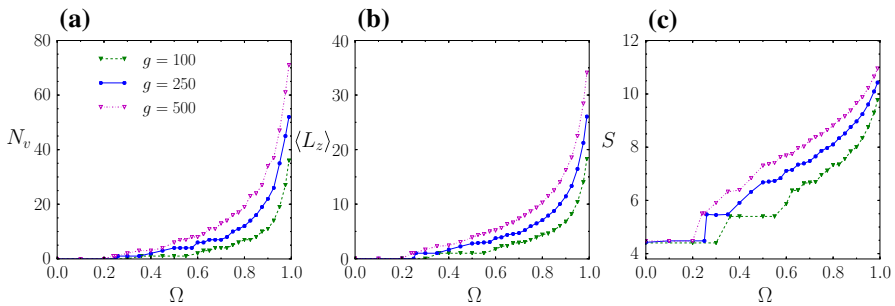


Fig. 4 **a** Number of vortices (N_v), **b** expectation value of angular momentum ($\langle L_z \rangle$), and **c** total entropy (S) with respect to rotation frequency Ω for different interaction strengths $g_{2D} = 100, 250$, and 500 (Color figure online)

the entropy as a function of Ω is shown in Fig. 5. Initially, total entropy S lies between S_{\max} and S_{\min} , but it diverges sharply after the vortex enters into the condensate, and becomes very close to the upper limit of S_{\max} .

Further, we calculate Λ , Δ , and Γ for the rotating condensate. In the rotating condensates, rotation frequency plays a crucial role in determining its properties. The critical rotation frequency decreases monotonically with increasing interaction strength for rotating BECs in all trap geometries [33,34]. The critical rotation frequency is gradually decreased with the increasing g_{2D} and is calculated for the interaction strengths, $g_{2D} = 100, 250$, and 500 are, $\Omega_c = 0.36, 0.26$, and 0.24 , respectively. When the rotation frequency is significantly higher than Ω_c , then more vortices enter into the condensate and form a triangular lattice [23]. We analyze the different regimes

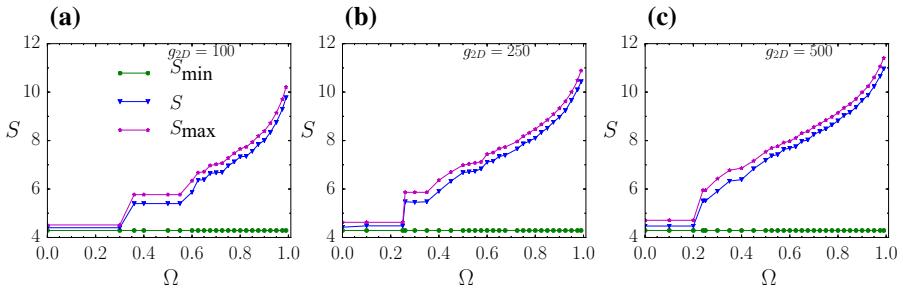


Fig. 5 Upper and lower limits of entropy compared with the total entropy of the system with respect to rotation frequency for several interaction strengths **a** $g_{2D} = 100$, **b** $g_{2D} = 250$, and **c** $g_{2D} = 500$. All quantities are dimensionless (Color figure online)

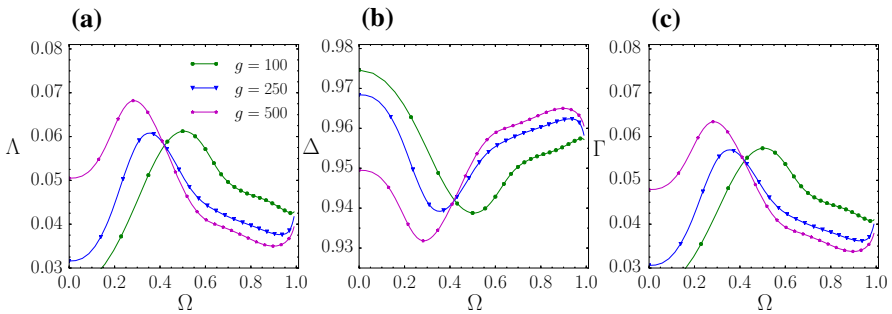
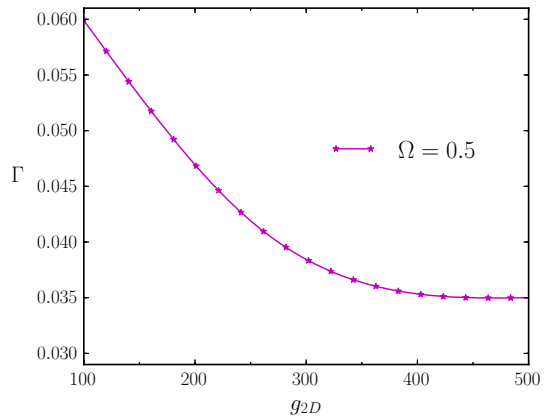


Fig. 6 **a** Order, **b** disorder and **c** complexity with respect to rotation frequency for the BECs with different interaction strengths. All quantities are dimensionless (Color figure online)

regarding the rotation frequency where we have no vortex or single vortex or many vortices. The order parameter Λ is plotted in Fig. 6a and shows that the order increases smoothly and shows a maximum value at critical rotation frequency $\Omega = \Omega_c$. Further, order decreases for $\Omega > \Omega_c$. On the other hand, in Fig. 6b, disorder shows the reverse behavior where disorder smoothly decreases till Ω_c and then it increases for $\Omega > \Omega_c$. Here, this reverse behavior is due to the entry of a large number of vortices into the condensate. They adjust themselves and fills up the disorder. From a thermodynamics point of view, it is an unexpected result that entropy rises and disorder falls. However, from our previous observation of nonrotating BEC, we conclude that till the critical frequency, entropy, and disorder are decoupled. Increasing the rotation frequency of the trap above Ω_c increases the dissipation in the condensate. Even though more vortices enter at $\Omega > \Omega_c$, they are not sufficient to fill up the disorder. So, disorder increases smoothly as a function of Ω . It assumes that for $\Omega > \Omega_c$, entropy and disorder are now coupled and it satisfies the most usual view of thermodynamics. In addition, we plot the complexity as a function of disorder parameter Ω in Fig. 6c. Complexity is minimum both for highest ordered and highest disordered state, but never reach to zero value. Thus, it is confirmed that the rotating condensate has been always complex. Complexity is increased by larger rotation frequency when the condensate has a large number of vortices. Similar to order, complexity Γ also exhibits a maximum

Fig. 7 Complexity as a function of interaction strengths show the complexity category III for the rotation frequency $\Omega = 0.5$, which is greater than critical rotation frequency for the interaction strength regime presented in this plot (Color figure online)



at Ω_c . So it confirms that the complexity belongs to category II. Rotating condensates exhibit two transitions. Disorder to order transition is continuing as far as $\Omega = \Omega_c$. In contrast, for $\Omega > \Omega_c$ the system shows a transition from order to disorder and complexity goes down with increasing interaction strength. Eventually, we chose a fixed rotation frequency $\Omega = 0.5$, which is the frequency greater than Ω_c of all the interaction strengths considered. The complexity as a function of disorder parameter g_{2D} for a fixed $\Omega = 0.5 > \Omega_c$ is plotted in Fig. 7. The complexity decreases with increasing interaction strength. We observe that the complexity goes down and the system exhibits category III complexity. From the above observations, we confirm the existence of category II and III complexities in rotating condensates.

4 Conclusion

In this work, we have presented the calculations of information entropy, order, disorder, and complexity for 2D rotating and nonrotating Bose–Einstein condensates. In order to study the order-disorder transition, we have derived the fundamental inequalities of entropy lower bound and upper bound for 2D quantum systems. We compare the total entropy of rotating and nonrotating 2D BECs with maximum and minimum limits of entropy. We observe that our system is unique which can exhibit all the three categories of complexity regarding SDL measure. We have considered the two-body interaction strength as a disorder parameter for the observations of complexity category in nonrotating condensates. In general, complexity is a monotonically increasing function regarding disorder parameter in a category I complexity. Similarly, in nonrotating BECs, complexity increases with disorder parameter which confirms the existence of the category I complexity.

Next, we have studied the entropy properties of rotating condensates. In the rotating condensates, we consider the rotation frequency as the disorder parameter when the interaction strength is fixed. The complexity increases until the rotation frequency reaches Ω_c ($\Omega = \Omega_c$). Then, complexity starts to decrease for $\Omega > \Omega_c$. The condensate becomes more dissipative due to the fast rotation and the entry of many vortices

that decrease the complexity. This transition in maximum and minimum complexity shows a hump at $\Omega = \Omega_c$. Thus, the characteristic corresponding to category II complexity is satisfied by the rotating condensate. Finally, the rotation frequency is unchanged and the interaction strength is used as a disorder parameter. In this setting, the complexity goes down regarding the increase in disorder parameter. This kind of decreasing complexity with respect to disorder parameter characterizes the existence of category III complexity in rotating condensates.

We believe that this is the first theoretical study performed in an experimentally realizable system which exhibits all three categories of complexity. Calculation of the complexity measure by LMC, their comparison with SDL and finding the value of α and β [18] for three types of complexity will be the subject of the future studies.

Acknowledgements RKK, BC, and AG acknowledge the support by FAPESP of Brazil under Grants 2014/01668-8, 2016/19622-0 and 2016/17612-7, respectively. AG also acknowledges the support by CNPq of Brazil.

Appendix A: Connection Between S_r, S_k with the Total Kinetic Energy T and Mean Square Radius in Two Dimensions

Maximum value of entropy in momentum space for a 2D system is given by

$$S_{k_\rho} \leq - \int n(\mathbf{k}_\rho) \ln n(\mathbf{k}_\rho) d\mathbf{k}_\rho. \tag{10}$$

Dimensionless form of kinetic energy $T = \frac{1}{2} \int n(\mathbf{k}_\rho) \mathbf{k}_\rho^2 d\mathbf{k}_\rho$, where $\mathbf{k}_\rho^2 = \mathbf{k}_x^2 + \mathbf{k}_y^2$. We consider the density in momentum space $n(\mathbf{k}_\rho) = A \exp[-\alpha \mathbf{k}_\rho^2]$, where A is the normalization constant and α is the appropriate Lagrange multiplier. The normalization of the density with respect to N particles is defined $\int_{-\infty}^{\infty} n(\mathbf{k}_\rho) d\mathbf{k}_\rho = N$. It calculates $A = \alpha N / \pi$ and $\alpha = N / 2T$. Thus, maximum value of the momentum space is given by Eq. (10) and further simplification yields the maximum value of momentum space entropy is given by

$$S_{k_\rho} \leq N(1 + \ln \pi) - N \ln N - N \ln \left(\frac{N}{2T} \right). \tag{11}$$

For the 2D model, we get the following relation from refs. [12,13],

$$S_\rho + S_{k_\rho} \geq 2N(1 + \ln \pi) - 2N \ln N. \tag{12}$$

From relations (11) and (12), we obtain the lower bound to S_ρ

$$S_\rho \geq N(1 + \ln \pi) - N \ln N + N \ln \left(\frac{N}{2T} \right). \tag{13}$$

Addition of (11) and (13) provides the lower bound to the excess information entropy in the position space over that in the momentum space.

$$S_\rho - S_{k_\rho} \geq 2N(1 + \ln \pi) - 2N \ln(2T). \quad (14)$$

Next, we calculate the upper as well as lower bounds for S_ρ and S_{k_ρ} , respectively, in terms of $\langle \rho^2 \rangle$

$$S_\rho \leq N(1 + \ln \pi) - 2N \ln N + N \ln \left(\langle \rho^2 \rangle \right), \quad (15)$$

where $\rho^2 = x^2 + y^2$ and

$$S_{k_\rho} \geq N(1 + \ln \pi) + 2N \ln N - N \ln \left(\langle \rho^2 \rangle \right). \quad (16)$$

For density distribution normalized to unity, the lower and upper limits of entropy in two dimensions took the form

$$S_{\rho \min} = (1 + \ln \pi) - \ln(2T), \quad (17a)$$

$$S_{\rho \max} = (1 + \ln \pi) + \ln \left(\langle \rho^2 \rangle \right), \quad (17b)$$

$$S_{k_\rho \min} = (1 + \ln \pi) - \ln \left(\langle \rho^2 \rangle \right), \quad (17c)$$

$$S_{k_\rho \max} = (1 + \ln \pi) + \ln(2T), \quad (17d)$$

$$S_{\min} = 2(1 + \ln \pi), \quad (17e)$$

$$S_{\max} = 2(1 + \ln \pi) + \ln \left(2 \langle \rho^2 \rangle T \right). \quad (17f)$$

References

1. S.R. Gadre, S.B. Sears, *J. Chem. Phys.* **71**, 432 (1979)
2. S.B. Sears, S.R. Gadre, *J. Chem. Phys.* **75**, 4626 (1981)
3. T. Koga, M. Morita, *J. Chem. Phys.* **79**, 1933 (1983)
4. N.L. Guevara, R.P. Sagar, R.O. Esquivel, *J. Chem. Phys.* **119**, 7030 (2003)
5. N.L. Guevara, R.P. Sagar, R.O. Esquivel, *J. Chem. Phys.* **122**, 084101 (2005)
6. R.P. Sagar, N.L. Guevara, *J. Chem. Phys.* **123**, 044108 (2005)
7. K.D. Sen, *J. Chem. Phys.* **123**, 074110 (2005)
8. P. Lambropoulos, D. Petrosyan, *Fundamentals of Quantum Optics and Quantum Information* (Springer, Berlin, 2007)
9. S.E. Massen, C.P. Panos, *Phys. Lett. A* **246**, 530 (1998)
10. S.E. Massen, C.P. Panos, *Phys. Lett. A* **280**, 65 (2001)
11. S.E. Massen, ChC Moustakidis, C.P. Panos, *Phys. Lett. A* **299**, 131–136 (2002)
12. I. Bialynicki-Birula, J. Mycielski, *Commun. Math. Phys.* **44**, 129 (1975)
13. S.R. Gadre, S.B. Sears, S.J. Chakravorty, R.D. Bendale, *Phys. Rev. A* **32**, 2602 (1985)
14. S.R. Gadre, R.D. Bendale, *Phys. Rev. A* **36**, 1932 (1987)
15. KCh. Chatzisavvas, ChC Moustakidis, C.P. Panos, *J. Chem. Phys.* **123**, 174111 (2005)
16. A. Saha, B. Talukdar, S. Chatterjee, *Phys. A* **474**, 370 (2017)
17. G.A. Sekh, A. Saha, B. Talukdar, *Phys. Lett. A* **382**, 315–320 (2018)
18. J.S. Shiner, M. Davison, P.T. Landsberg, *Phys. Rev. E* **59**, 1459 (1999)

19. T. Sriraman, B. Chakrabarti, A. Trombettoni, P. Muruganandam, J. Chem. Phys. **147**, 044304 (2017)
20. C.P. Panos, Phys. Lett. A **289**, 287 (2001)
21. P.T. Landsberg, J.S. Shiner, Phys. Lett. A **245**, 228 (1998)
22. M.B. Kim, A. Svidzinsky, G.S. Agarwal, M.O. Scully, Phys. Rev. A **97**, 013605 (2018)
23. A.L. Fetter, A.A. Svidzinsky, J. Phys. Condens. Matter **13**, R135 (2001)
24. A.L. Fetter, A.A. Svidzinsky, Int. J. Mod. Phys. B **19**, 1835 (2005)
25. A.L. Fetter, Rev. Mod. Phys. **81**, 647 (2009)
26. C.J. Pethick, H. Smith, *Bose–Einstein Condensation in Dilute Gases* (Cambridge University Press, Cambridge, 2002)
27. N.P. Proukakis, D.W. Snoke, P.B. Littlewood, *Universal Themes of Bose–Einstein Condensation* (Cambridge University Press, Cambridge, 2017)
28. M.R. Matthews, B.P. Anderson, P.C. Haljan, D.S. Hall, C.E. Wieman, E.A. Cornell, Phys. Rev. Lett. **83**, 2498 (1999)
29. A.E. Leanhardt, A. Görlitz, A.P. Chikkatur, D. Kielpinski, Y. Shin, D.E. Pritchard, W. Ketterle, Phys. Rev. Lett. **89**, 190403 (2002)
30. Y.J. Lin, R.L. Compton, K. Jimenez-Garcia, J.V. Porto, I.B. Spielman, Nature **462**, 628 (2009)
31. K.W. Madison, F. Chevy, W. Wohlleben, J. Dalibard, Phys. Rev. Lett. **84**, 806 (2000)
32. K.W. Madison, F. Chevy, V. Bretin, J. Dalibard, Phys. Rev. Lett. **86**, 4443 (2001)
33. D.L. Feder, C.W. Clark, B.I. Schneider, Phys. Rev. Lett. **82**, 4956 (1999)
34. D.L. Feder, C.W. Clark, B.I. Schneider, Phys. Rev. A **61**, 011601(R) (1999)
35. R.K. Kumar, P. Muruganandam, Eur. Phys. J. D **68**, 289 (2014)
36. R.K. Kumar, T. Sriraman, H. Fabrelli, P. Muruganandam, A. Gammal, J. Phys. B At. Mol. Opt. Phys. **49**, 155301 (2016)
37. R.K. Kumar, L. Tomio, B.A. Malomed, A. Gammal, Phys. Rev. A **96**, 063624 (2017)
38. W. Bao, H. Wang, P.A. Markowich, Commun. Math. Sci. **3**, 55 (2005)
39. M.C. Tsatsos, A.U.J. Lode, J. Low Temp. Phys. **181**, 171 (2015)
40. C.P. Panos, KCh. Chatzisavvas, ChC Moustakidis, E.G. Kyrkou, Phys. Lett. A **363**, 78 (2007)
41. R.G. Catalán, J. Garay, R. López-Ruiz, Phys. Rev. E **66**, 011102 (2002)
42. J.C. Angulo, J. Antolín, J. Chem. Phys. **128**, 164109 (2008)
43. R. López-Ruiz, H.L. Mancini, X. Calbet, Phys. Lett. A **209**, 321 (1995)
44. C.P. Panos et al., in *Statistical complexity: applications in electronic structure*, ed. by K.D. Sen (Springer, Dordrecht, 2011)
45. A. Gammal, T. Frederico, L. Tomio, Phys. Rev. A **64**, 055602 (2001)
46. A. Gammal, L. Tomio, T. Frederico, Phys. Rev. A **66**, 043619 (2002)
47. M. Brtko, A. Gammal, L. Tomio, Phys. Lett. A **359**, 339 (2006)
48. P. Muruganandam, S.K. Adhikari, Comput. Phys. Commun. **180**, 1888 (2009)
49. D. Vudragović, I. Vidanović, A. Balaž, P. Muruganandam, S.K. Adhikari, Comput. Phys. Commun. **183**, 2021 (2012)
50. H.A. Van der Vorst, J. Sci. Stat. Comput. **13**(2), 631 (1992)
51. J. Yang, J. Comput. Phys. **228**, 7007 (2009)
52. D.A. Butts, D.S. Rokhsar, Nature **397**, 327 (1999)